UDC 551.515.21

# COMPARISONS OF TROPICAL CYCLONE SIMULATIONS WITH AND WITHOUT THE ASSUMPTION OF CIRCULAR SYMMETRY

RICHARD A. ANTHES, JAMES W. TROUT, and STANLEY L. ROSENTHAL

National Hurricane Research Laboratory, Environmental Research Laboratories, NOAA, Miami, Fla.

## ABSTRACT

Results from a three-layer asymmetric hurricane model previously described by the authors are compared with results from an axially symmetric analog to investigate the effect of the symmetry assumption on the internal dynamics of model cyclones. The symmetric model storm initially develops more rapidly than the asymmetric storm. The differences in intensity during the first 100 hr are related to differences in horizontal resolution produced by the staggered grid used with the symmetric model. The symmetric model, on the other hand, does not produce the second period of intensification that starts at 120 hr in the asymmetric model. This fact supports the conclusion reached in the earlier paper that the development of large-scale asymmetries at 100 hr is closely related to the subsequent intensification.

Although the life cycles of the two storms are different, the azimuthally averaged structure of the asymmetric storm at maximum intensity is similar to the corresponding structure of the symmetric model storm and supports the adequacy of symmetric models in investigating many aspects of tropical cyclone structure.

## 1. INTRODUCTION

Preliminary results from an asymmetric model have simulated the characteristic features of the tropical cyclone with a surprising degree of realism in spite of the coarse horizontal (30 km) and vertical (three layers) resolution (Anthes et al. 1971, hereafter designated ART). In particular, this model reproduced spiral rainbands and the strongly asymmetric structure of the outflow layer. Although realistic results with axisymmetric models have been obtained by a number of authors (Yamasaki 1968, Ooyama 1969, Rosenthal 1970, Sundqvist 1970), the symmetry assumption, at first glance, appears to be rather severe. An important area of investigation is, therefore, the effect of the symmetry assumption on the internal dynamics of the model cyclone. Comparison between results obtained from symmetric and asymmetric models which are otherwise similar is a potential tool in this area of investigation.

The primary purpose of this paper is to compare results of the asymmetric model (ART) with results from an axially symmetric analog model which is nearly identical. A secondary objective is to briefly summarize experiments with this symmetric model which were helpful in the design of the asymmetric model. The next section describes the numerical framework of the symmetric analog with particular emphasis on the differences between it and the asymmetric model. The major differences are the use of polar rather than Cartesian coordinates and the horizontal staggering of variables, which is a feature of the symmetric model but not of the asymmetric model.

## 2. DESIGN OF THE SYMMETRIC MODEL

### A. BASIC EQUATIONS

The equations of motion in the $\sigma$-coordinate system (Phillips 1957) under the assumption of axial symmetry may be written

$$\frac{\partial p^*u}{\partial t}=-\frac{1}{r}\frac{\partial}{\partial r}(rp^*u^2)+\frac{p^*v^2}{r}-p^*\frac{\partial\dot{\sigma}u}{\partial\sigma}+fvp^* -p^*\frac{\partial\phi}{\partial r}-RT\frac{\partial p^*}{\partial r}+\frac{1}{r^2}\frac{\partial}{\partial r}\left[K_Hr^3\frac{\partial}{\partial r}\left(p^*\frac{u}{r}\right)\right]+F_V(u) \quad (1)$$

and

$$\frac{\partial p^*v}{\partial t}=-\frac{1}{r}\frac{\partial}{\partial r}(rp^*uv)-\frac{p^*uv}{r}-p^*\frac{\partial\dot{\sigma}v}{\partial\sigma}-fup^* +\frac{1}{r^2}\frac{\partial}{\partial r}\left[K_Hr^3\frac{\partial}{\partial r}\left(p^*\frac{v}{r}\right)\right]+F_V(v). \quad (2)$$

The symbols $u$ and $v$ are the velocity components in the radial ($r$) and tangential ($\lambda$) directions respectively, $p^*$ is the surface pressure, $\sigma=p/p^*$, where $p$ is pressure and $\dot{\sigma}$ is the vertical velocity in the $\sigma$-system. The symbol $\phi$ denotes the geopotential of a $\sigma$-surface, $T$ is temperature, and $R$ is the gas constant for dry air. The Coriolis parameter, $f$, is $5\times10^{-5}$ s$^{-1}$ and is appropriate to approximately 20°N. Terms involving $K_H$ (the horizontal eddy viscosity coefficient) represent the horizontal diffusion of momentum, and the terms involving $F_V$ represent vertical eddy diffusivity of momentum. These are discussed later.

The continuity and thermodynamic equations are

$$\frac{\partial p^*}{\partial t}=-\frac{1}{r}\frac{\partial}{\partial r}(rp^*u)-\frac{\partial p^*\dot{\sigma}}{\partial\sigma} \quad (3)$$

and

$$\frac{\partial p^*T}{\partial t}=-\frac{1}{r}\frac{\partial}{\partial r}(rp^*uT)-p^*\frac{\partial\dot{\sigma}T}{\partial\sigma}+\frac{RT\omega}{c_p\sigma} +\frac{p^*}{c_p}\dot{Q}+\frac{p^*K_T}{r}\frac{\partial}{\partial r}\left(r\frac{\partial T}{\partial r}\right) \quad (4)$$

where $\dot{Q}$ is the diabatic heating per unit mass, $c_p$ is the specific heat at constant pressure, and $\omega=dp/dt$ is related

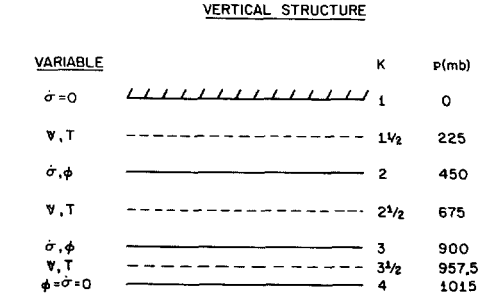


FIGURE 1.—Vertical information-levels for symmetric and asymmetric models.

to $\dot{\sigma}$ by

$$\omega=p^*\dot{\sigma}+\sigma\frac{dp^*}{dt}. \tag{5}$$

The term involving the thermal diffusivity for heat, $K_T$, represents the lateral diffusion of heat due to the presence of subgrid-scale eddies. The hydrostatic equation in the $\sigma$-system is

$$\frac{\partial\phi}{\partial\sigma}=-\frac{RT}{\sigma}. \tag{6}$$

Except for the assumption of symmetry and the use of polar coordinates, these are the equations used by Smagorinsky et al. (1965) for general circulation studies and those used in ART for the asymmetric hurricane model.

### B. STRUCTURE OF THE SYMMETRIC MODEL

The vertical structure of the model (fig. 1) is identical to that of the asymmetric model and features upper and lower tropospheric layers of equal pressure depth and a thinner Ekman boundary layer. The information levels for the dynamic and thermodynamic variables are staggered according to the scheme used by Kurihara and Holloway (1967). The horizontal mesh, however, differs significantly from that for the asymmetric model. To avoid the singularity at the origin of the polar coordinate system, the thermodynamic variables, including $p^*$, $T$, $\dot{Q}$, $\dot{\sigma}$, and $\omega$, are forecast at grid points halfway between the prediction points for the momentum variables, as in previous symmetric models (Yamasaki 1968, Ooyama 1969, Rosenthal 1970). While identical horizontal grids in the symmetric and asymmetric models would be desirable for purposes of comparison, the alternative of defining the thermodynamic and momentum variables at the same points in the symmetric analog would yield additional computational differences at the singularity, $r=0$. Difference in results due to this effect would make comparisons with the asymmetric model as difficult as is presently the case. Finally, it is important to isolate and explain differences due to the horizontal grid systems since the vast majority of previous symmetric hurricane experiments have utilized the staggered grid system. Since the motion vanishes at $r=0$ because of the symmetry condition, no computations are required at the pole. The pressure-weighted horizontal velocity components, $up^*$ and $vp^*$ are thus forecast at the radii

$$r_j=(j-1)\Delta r, \qquad j=2, 3, \ldots, \tag{7}$$

while the remaining variables are calculated at the radii

$$r_j=(j-\tfrac{1}{2})\Delta r, \qquad j=1, 2, \ldots. \tag{8}$$

This grid staggering is the major numerical difference between the two models and results in a smaller truncation error when horizontal derivatives are estimated. As we will see below, differences in truncation error are a major factor in determining the differences in the behavior of the two models.

### C. THE FINITE-DIFFERENCE EQUATIONS

The finite-difference equations for the symmetric model are summarized very briefly in this section; in most cases, the equations are straightforward analogs to those described in ART. We adopt Shuman and Stackpole's (1968) finite-difference notation and write

$$\alpha_r=\frac{\alpha_{j+1/2}-\alpha_{j-1/2}}{\Delta r}$$

and (9)

$$\overline{\alpha}^r=(\alpha_{j+1/2}+\alpha_{j-1/2})/2$$

where $j$ is the radial index.

For vertical differences and averages, we define

$$\overline{\alpha}^\sigma=(\alpha_{k+1/2}+\alpha_{k-1/2})/2$$

and (10)

$$\delta\alpha=(\alpha_{k+1/2}-\alpha_{k-1/2})$$

where $k$ is the vertical index.

The horizontal portion of the difference scheme is similar to the scheme utilized for the asymmetric model with allowance made for the horizontal staggering of the variables. The vertical differencing is identical to that in the asymmetric model.

By use of the operators [eq (9) and (10)], the equations of motion can be expressed in the form

$$\frac{\partial p^*u}{\partial t}=-\frac{1}{r}(\overline{rup^*}^r\overline{u}^r)_r-p^*\frac{\delta\dot{\sigma}\overline{u}^\sigma}{\delta\sigma}-\overline{p^*}^r\overline{\phi}^\sigma_r$$
$$-R\overline{T}^r p^*_r+\frac{1}{r^2}\left[K_H r^3\left(\frac{p^*u}{r}\right)_r\right]_r \tag{11}$$

and

$$\frac{\partial p^*v}{\partial t}=-\frac{1}{r}(\overline{rup^*}^r\overline{v}^r)_r-p^*\frac{\delta\dot{\sigma}\overline{v}^\sigma}{\delta\sigma}+\frac{1}{r^2}\left[K_H r^3\left(\frac{p^*v}{r}\right)_r\right]_r \tag{12}$$

which are applied at the half levels. The continuity equation takes the form

$$\frac{\partial p^*}{\partial t}=-\frac{1}{r}(rup^*)_r-p^*\frac{\delta\dot{\sigma}}{\delta\sigma} \tag{13}$$

and is also applied at the half levels. The vertical sum of eq (13), subject to the boundary conditions $\dot{\sigma}=0$ at $\sigma=0$ and $\sigma=1$, is used to compute $\partial p^*/\partial t$. Equation (13) is then used to compute $\dot{\sigma}$ at the integral levels. The thermodynamic equation, also applied at the half levels, is

written

$$\frac{\partial p^*T}{\partial t}=-\frac{1}{r}(p^*u\overline{T}^r)_r-p^*\frac{\delta\dot{\sigma}\overline{T}^\sigma}{\delta\sigma}+\frac{RT\omega}{c_p\sigma}+\frac{p^*}{c_p}\dot{Q}+\frac{p^*K_T}{r}(rT_r)_r. \quad (14)$$

The symbol $\overline{T}^\sigma$ denotes a temperature at the integral levels computed by linear interpolation of *potential* temperature over $\sigma$ between adjacent half levels.

The quantity $\omega=dp/dt$ is defined at the half levels and computed from

$$\omega=p^*\dot{\sigma}^\sigma+\overline{\sigma}^\sigma\left[\frac{\partial p^*}{\partial t}+\overline{u(p^*)_r}^r\right]. \quad (15)$$

The hydrostatic equation in the form

$$\frac{\delta\phi}{\delta\sigma}=-\frac{RT}{\overline{\sigma}^\sigma} \quad (16)$$

is also applied at the half levels. The horizontal velocity components are computed from

$$u=\frac{p^*u}{\overline{p^*}^r};\qquad v=\frac{p^*v}{\overline{p^*}^r}. \quad (17)$$

### D. COMPARISON OF HORIZONTAL TRUNCATION ERROR IN THE SYMMETRIC AND ASYMMETRIC MODELS

As already noted, a significant difference in the computational aspects of the asymmetric model and its two-dimensional analog is the difference in truncation errors caused by the staggering of variables in the symmetric model. This appears to be especially important in the computation of the pressure gradient terms.

The finite-difference analog to the east-west component of pressure gradient force (PGF) for the asymmetric model is

$$(\mathrm{PGF})_{\mathrm{ASYM}}\approx-p^*\overline{\phi_r}^{\sigma r}-RT\overline{(p^*)_r}^r \quad (18)$$

while the corresponding term for the symmetric model is

$$(\mathrm{PGF})_{\mathrm{SYM}}\approx-\overline{p^*}^r\overline{\phi_r}^\sigma-R\overline{T}^r p^*_r. \quad (19)$$

The pressure differences are evaluated over 60-km intervals in the asymmetric model, compared to 30-km intervals in the symmetric analog; thus, the symmetric model will resolve the intense pressure gradients that are typical of hurricanes with greater accuracy than will the asymmetric model.

The importance of this effect may be shown by a simple example. Consider the evaluation of the pressure gradient for a symmetric pressure field utilizing the finite-difference schemes for the asymmetiic and symmetric models.[1] For this example, consider the following function that is similar to the shape of pressure profiles in hurricanes:

$$p(r)=-(1+ar)e^{-ar} \quad (20)$$

[1] This analysis is directly pertinent for comparison of the symmetric model results and the results from the first 120 hr of the asymmetric model when the model storm is quite symmetric (see ART).

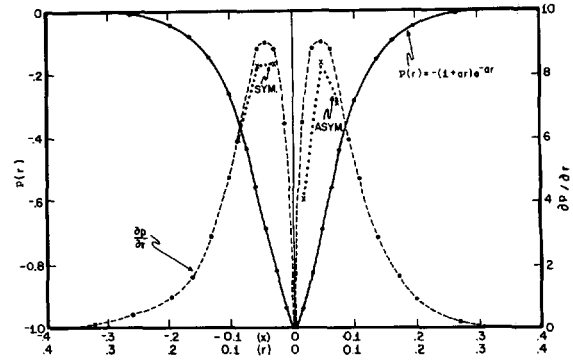


FIGURE 2.—Hurricanelike pressure profile through the symmetric-vortex center and finite-difference estimates of pressure gradient corresponding to symmetric and asymmetric model evaluations. Note that the maximum pressure gradient estimate for the asymmetric model occurs at a larger distance from the vortex center than does the estimate for the symmetric model.

and

$$\frac{\partial p}{\partial r}=a^2re^{-ar}. \quad (21)$$

The graphs of $p(r)$ and its radial derivative are shown in figure 2 for $a=25$ and a nondimensional $r$ ranging from 0 to 0.4. (For a rough comparison with the hurricane scale, $r$ may be multiplied by 1000 km.) Figure 2 also shows the finite-difference estimates for $\partial p/\partial r$ computed over 0.060 units of $r$ at points 0.015, 0.045, and 0.075 (corresponding to the evaluation for the asymmetric model); and the estimates computed over 0.030 units of $r$ at points 0.030, 0.060, and 0.090 (corresponding to the evaluation for the symmetric model). Large differences between the estimates occur at the first grid point from the center. While the maximum gradient for the symmetric model occurs at $r=$ 0.030 (the grid point closest to the center), the maximum gradient in the asymmetric model is displaced to the second grid point from the center ($r=0.045$) and is underestimated by a factor of 2 at $r=0.015$. This is due to the large grid increment which requires pressure values on the opposite side of the pressure minimum. Thus, for a hurricanelike pressure field, the asymmetric model, in comparison with the symmetric model, significantly underestimates the pressure gradient close to the center. As we shall see, this results in a considerably weaker storm during the earlier portions of the asymmetric integration.

### E. VERTICAL DIFFUSION OF MOMENTUM

The terms $F_V(v)$ and $F_V(u)$, which appear in eq (1) and (2), represent diffusive and "frictional" effects due to vertical transports of horizontal momentum by subgrid eddies smaller than the cumulus scale and include the important surface drag. These terms are identical in form to those in the asymmetric model (ART) and, hence, are not presented here.

### F. TIME INTEGRATION

As in the asymmetric model, the Matsuno (1966)

simulated forward-backward scheme is used for time integration. The criteria for linear computational stability is primarily determined by the external gravity wave. While a time step of 60 s was adequate for the asymmetric model, the evaluation of horizontal divergence in eq (13) over intervals of 30 km in the symmetric version necessitated a smaller time step of 40 s.

### G. LATERAL BOUNDARY CONDITIONS

The small domain size (450 km radius) makes the choice of lateral boundary conditions extremely important. Preliminary experimentation showed that realistic results could be obtained for boundary conditions similar to those employed in other symmetric models (Anthes 1970, Rosenthal 1970). These boundary conditions require the pressure and temperature gradients, the horizontal divergence, and the relative vorticity to vanish. The zero divergence assumption and the finite-difference formulation [eq (13)] for the continuity equation imply that the pressure at the lateral boundary is steady state, as is also the case for the asymmetric model. The boundary condition on temperature for the symmetric model, however, allows the temperature on the boundary to change, unlike the steady-state temperatures on the boundary of the asymmetric model. This second difference is probably less important than that due to the horizontal grids since temperatures at the boundary of the symmetric analog change by no more than 1°C during experiments.

### H. DIABATIC EFFECTS

As in ART, this preliminary experiment does not contain an explicit water cycle and the convective adjustments of macroscale temperature are parameterized as they were in the original version of Rosenthal's (1969) symmetric model. The basic characteristics of this convective adjustment, summarized in ART, are not repeated here.

The heating function, previously written for the $z$-system (Rosenthal 1969), may be expressed in the $\sigma$-system as follows. Let

$$I=\frac{-L[(\nabla\cdot p^*\mathbf{V}q)\delta\sigma]_{k=7/2}}{\sum_{k=1}^{3}(T_c-T)_k\delta\sigma} \tag{22}$$

where $T_c$ is the temperature along the pseudoadiabat with the equivalent potential temperature of the $\sigma=1$ surface; $q$ is the specific humidity; $L$ is the latent heat of vaporization. Then,

$$p^*\dot{Q}=I(T_c-T) \tag{23}$$

if $I>0$ and $(\nabla\cdot p^*\mathbf{V}q)_{k=7/2}<0$.

Otherwise,

$$p^*\dot{Q}=0. \tag{24}$$

In finite-difference form,

$$(\nabla\cdot p^*\mathbf{V}q)_{k=7/2}=[(up^*\bar{q}^r)_r]_{k=7/2}. \tag{25}$$

The parameterization of nonconvective latent heat release under nearly moist adiabatic conditions, under which $T_c\approx T$, proceeds as follows. Whenever $(T_c-T)\leq 0.5$°C at $k=3/2$ or 7/2, this quantity is arbitrarily set to 0.5°C. Under a nearly moist adiabatic lapse rate, therefore, $T_c-T=0.5$°C at both levels, and the latent heat is partitioned equally between the upper and lower troposphere. From eq (23), therefore, latent heat is released in the column as long as a water vapor supply from the boundary layer is present.

The value of $q_{k=7/2}$, needed for the evaluation of eq (22), is assumed to be given by

$$q_{7/2}=\min\begin{Bmatrix}0.90\,q_s\\0.020\end{Bmatrix} \tag{26}$$

where $q_s$ is the saturation specific humidity.

The surface temperature, $T^*$, and specific humidity, $q^*$, required to establish the pseudoadiabat appropriate to parcel ascent from the surface are computed, as in the asymmetric model, by downward extrapolation from the $k=7/2$ level,

$$T^*=T_{k=7/2}+3.636\text{°K} \tag{27}$$

and

$$q^*=0.90\,q_s(T^*,p^*). \tag{28}$$

The formulation of the air-sea exchange of sensible heat is identical to that used in ART.

### I. INITIAL CONDITIONS

The initial conditions consist of a vortex in gradient balance. The temperatures at the levels $k=3/2$, 5/2, and 7/2 are taken from a mean tropical atmosphere (Hebert and Jordan 1959). The initial surface pressure (in mb) is then defined by

$$\begin{aligned}&p^*=1011.0-4.0\cos\left(\frac{\pi}{375}r\right), && r<375\text{ km}\\ &\text{and}\\ &p^*=1015.0 && r\geq 375\text{ km}\end{aligned} \tag{29}$$

where $r$ is given in kilometers.

The initial geopotentials of the $\sigma$-surfaces are calculated by an upward integration of the hydrostatic equation. To obtain the initial wind field, we write the gradient wind equation for the $\sigma$-system as

$$\frac{v^2}{r}+fv=\frac{RT}{p^*}\frac{\partial p^*}{\partial r}+\frac{\partial\phi}{\partial r}. \tag{30}$$

The pressure field [eq (29)], together with the specified temperature field, yields a maximum gradient wind at the $k=7/2$ level of 18 m/s at a radius of 240 km. Although these conditions represent a rather strong vortex, two experiments, to be briefly discussed later, showed the mature state of the storm to depend very little on the strength of the initial vortex. The time of development, on the other hand, varied from 6 days to 1 day depending on the strength of the initial circulation. Therefore, a computational economy is realized by increasing the strength of the initial vortex.

## 3. EXPERIMENTAL RESULTS

### A. VARIATIONS IN INITIAL CONDITIONS AND LATERAL MIXING TERMS

One of the objectives of this paper is to present results

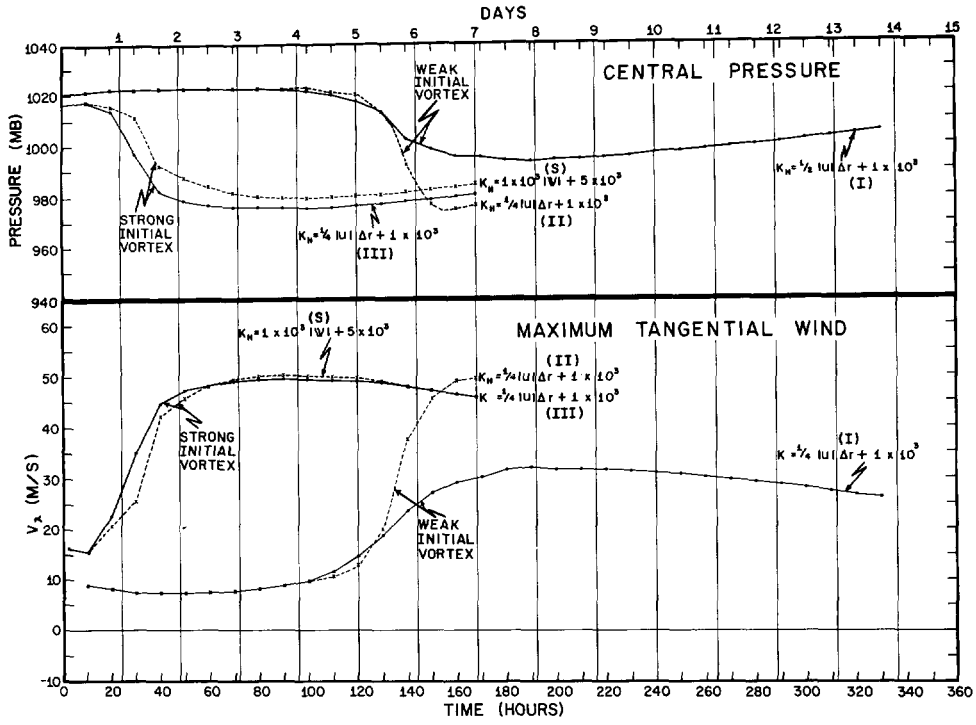


FIGURE 3.—Summary of four experiments with the symmetric analog model. Experiments I and II start with a weak initial vortex and compare two formulations of the horizontal eddy viscosity coefficient. Experiments labeled III and S start with a stronger initial vortex. The experiment labeled S is most nearly similar to the asymmetric model experiment and serves as the basis for comparison.

from the symmetric model that were useful in the design of the asymmetric model. The first series of experiments provided useful information regarding the formulation of the horizontal eddy diffusivity for momentum ($K_H$) and the effect of the strength of the initial vortex on the life cycle of the model storm.

Figure 3 contains the time variation of minimum pressure and maximum wind speeds for four of the more significant symmetric model experiments. The profiles marked "S" denote the symmetric experiment that is most similar to the asymmetric experiment described in ART and will serve as the basis for a detailed comparison in the next section.

These experiments suggested the form for the variable horizontal eddy diffusivity of momentum that was ultimately adopted for the asymmetric model and which may be written

$$K_H=c_1|\mathbf{V}|+c_2 \tag{31}$$

where $c_1=1.0\times10^3$m and $c_2=5\times10^3\text{m}^2\cdot\text{s}^{-1}$. A number of experiments showed that constant values of $K_H$ were unacceptable because values small enough to allow the initial vortex to intensify provided too little diffusion in the more intense mature stage. Conversely, values large enough for an intense circulation yielded an overdamping in the early stages to the extent that intensification was unable to take place. Experiments with Smagorinsky's (1965) variable $K_H$ (proportional to the magnitude of the total deformation of the horizontal motion) gave unrealistic velocity fields near the storm center.

Encouraged by results obtained from symmetric models (Rosenthal 1970, Yamasaki 1968) in which upstream differencing provided an implicit diffusion coefficient proportional to the advecting velocity, a coefficient of the form

$$K_H=c_3|u|\Delta r+c_4 \tag{32}$$

was tested with the symmetric analog. This formulation yields the required compromise between values small enough to allow storm development and large enough to provide realistic structures in the intense mature state. Equation (31) which was utilized in the asymmetric model represents a generalization of eq (32) to two horizontal dimensions in which both horizontal velocity components are advecting components.

Figure 3 shows three experiments with the $K_H$ formulation given by eq (32). The curves labeled I and II represent experiments which are identical except for the value of the proportionality constant $c_3$. For $c_3=\frac{1}{2}$ (case I) the lowest pressure and maximum tangential wind speed of the storm are 994 mb and 33 m/s, respectively, typical of a weak hurricane. For $c_3=\frac{1}{4}$ (case II) the minimum central pressure is 975 mb and the maximum tangential wind is 50 m/s, representative of a moderate hurricane. The evolution of both experiments is similar, with both storms beginning a very slow filling process shortly after reaching maximum intensity.

The "organization phase" of 6 days in experiments I and II is typical of hurricane models that start with a weak vortex. It is computationally uneconomical, however, especially with three-dimensional models, to devote 6 days to the relatively uninteresting stage of gradual intensification. Experiment III represents an effort to shorten this phase, and is identical to experiment II except that the initial pressure perturbation in experiment III is twice the

amplitude of that in experiment II. These conditions, given by eq (29), are identical to those used for the asymmetric calculation. A comparison of curves II and III reveals that the mature stages of both experiments have nearly the same intensity. The structures (not shown) are also quite similar, indicating that the major effect of the strength of the initial vortex is on the early growth rate rather than on the final stage of the storm.

The structures of the experiments utilizing a $K_H$ of the form given in eq (32) were all quite reasonable compared to empirical data. As already noted, the generalization of eq (32) to two horizontal dimensions suggests the utilization of the total wind rather than the inflow component alone. Thus, in eq (31), the variable part of $K_H$ is made proportional to the wind speed. This formulation, with $c_1=1\times10^3$ m and $c_2=5\times10^3$ m$^2$ • s$^{-1}$, gave results which were comparable to those obtained by eq (32). This experiment, designated S in figure 3, is the basis for comparison of the symmetric and asymmetric models in the next section.

### B. COMPARISON OF SYMMETRIC AND ASYMMETRIC MODEL RESULTS

Figure 4 compares the maximum wind speed in the boundary layer with the minimum surface pressure for the symmetric and asymmetric experiments. Results for the first 24 hr are nearly identical. After this time, however, significant differences develop. At about 40 hr, the asymmetric model reaches a near steady state that closely resembles a weak hurricane. The symmetric model storm, however, intensifies at a faster rate and deepens until a considerably stronger steady state is reached at about 100 hr.

Thereafter, the symmetric storm fills and the computation is terminated at 165 hr. The asymmetric model, on the other hand, remains in a weak quasi-steady state until 120 hr when a second period of intensification begins. This second deepening phase, as discussed in ART, seems to be related to the appearance at this time of large-scale asymmetries, notably in the outflow layer.

During the first 120 hr the differences between the symmetric and asymmetric model storms are striking. They are not, however, directly attributable to differences in storm symmetry, since the asymmetric model storm remains very nearly circularly symmetric for the first 100 hr or so. The differences appear to be related to the differences in horizontal grid structure and truncation error discussed in section 2D. Apparently, the better resolution of the pressure gradient force that results from the grid staggering in the symmetric model produces a stronger pressure gradient, increased inflow, and consequently increased tangential winds. This indicates that the nonstaggered 30-km resolution of the asymmetric model severely limits the early development of the storm.

In ART, it was shown that the second period of intensification in the asymmetric experiment was related to the development of a form of inertial (or dynamic) instability that leads to the growth of asymmetric perturbations. This type of instability cannot be released in the symmetric model and possibly explains why the symmetric model does not exhibit two stages of deepening. On the other hand, a symmetric vortex can exhibit an inertial instability for horizontal symmetric ring displacements if

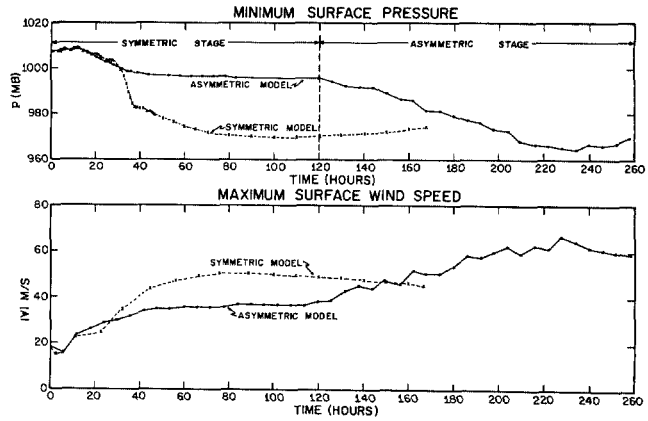


FIGURE 4.—Time variation of the minimum surface pressure and the maximum surface wind speed for the symmetric and asymmetric model experiments.

$$\left(\frac{\partial v}{\partial r}+\frac{v}{r}+f\right)\left(\frac{2v}{r}+f\right)<0. \tag{33}$$

The tentative conclusion reached in ART was that this instability played no significant role in either phase of the deepening since it was not present during the first phase and since the second phase was highly asymmetric. In previous studies with symmetric models, similar conclusions have been reached by Ooyama (1969) and Rosenthal (1969). The behavior of the symmetric analog discussed here appears to directly support this conclusion, and it indirectly supports the conclusions reached in ART regarding the importance of asymmetric inertial instabilities during the second period of deepening in the asymmetric model.

Figure 5 shows the time variation of minimum upper tropospheric relative vorticity for the symmetric and asymmetric models. The relative vorticity in the symmetric model reaches a minimum value of $-6\times10^{-5}$ s$^{-1}$ *after* the intensification has occurred. Since $f=5\times10^{-5}$ s$^{-1}$, the absolute vorticity is positive until the intensification is nearly complete, and remains nearly zero thereafter. For the symmetric model, the second factor in eq (33), $[(2v/r)+f]$, is always positive. It would appear, therefore, that this instability is *not* a factor in the development of the symmetric model storm. For the asymmetric model, the vorticity shown by figure 5 contains the asymmetric component of the wind as well as the symmetric component. These values, therefore, are not applicable to the type of instability represented by eq (33); rather they must be applied to the type of instability discussed in ART that leads to the growth of asymmetric perturbations.

Figure 6 shows the temporal variations of the components of the kinetic energy budget. The sum of (1) the conversion of potential to kinetic energy, [C($K$)], (2) the flux of kinetic energy across the lateral boundary, [B($K$)],

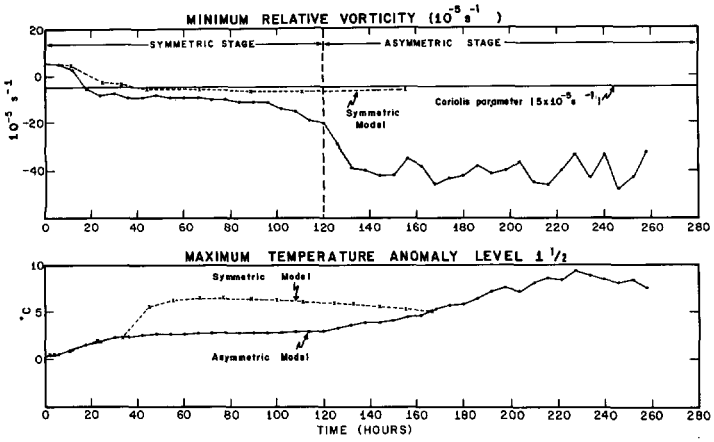


FIGURE 5.—Time variation of (A) the minimum relative vorticity in the upper troposphere and (B) the maximum temperature anomaly in the upper troposphere, for the symmetric and asymmetric model experiments.

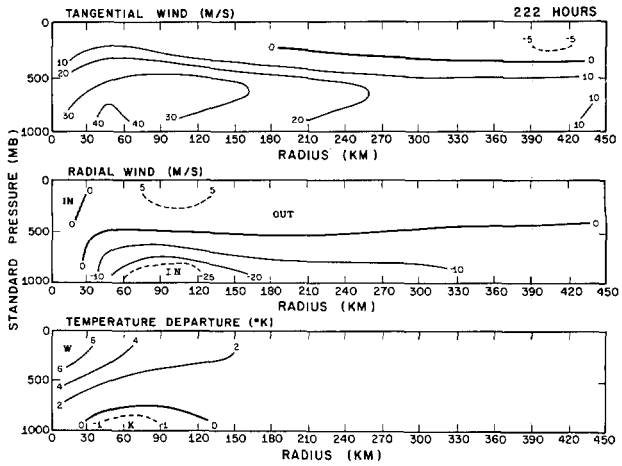


FIGURE 7.—Azimuthal mean vertical cross sections for the tangential wind, the radial wind, and the temperature anomaly at 222 hr for the asymmetric model experiment.

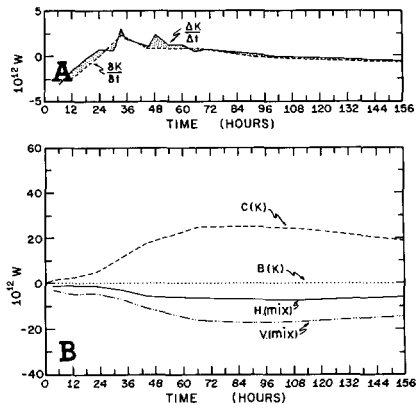


FIGURE 6.—(A) time variation of the observed kinetic energy change and of the change computed from the kinetic energy equation, (B) time variation of individual components of the kinetic energy tendency: C($K$) is the conversion of potential to kinetic energy, B($K$) is the flow of kinetic energy through the lateral boundary, H($mix$) is the loss of kinetic energy through lateral eddy viscosity, V($mix$) is the loss of kinetic energy through vertical eddy viscosity and includes the effect of surface drag friction. Both (A) and (B) are for the symmetric model.

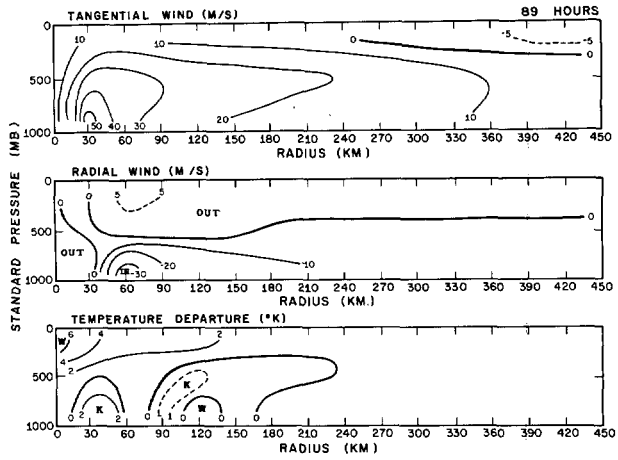


FIGURE 8.—Vertical cross sections for the tangential wind, the radial wind, and the temperature anomaly at 89 hr for the symmetric model experiment.

(3) the dissipation due to lateral mixing, [H($mix$)], and (4) the dissipation due to vertical mixing, [V($mix$)] equals the "analytic" kinetic energy tendency ($\partial K/\partial t$). Also shown by figure 6 are the observed rates of change of kinetic energy, ($\Delta K/\Delta t$). The difference between $\partial K/\partial t$ and $\Delta K/\Delta t$ is a measure of the truncation error and, as figure 6 shows, this difference is quite small. Furthermore, the individual components of the budget are reasonable when compared to empirical estimates (Hawkins and Rubsam 1968, Miller 1962, Palmén and Riehl 1957, Riehl and Malkus 1961).

Comparison of the energy budgets for the symmetric and asymmetric model storms for the same intensity (as measured by minimum pressure) shows that the individual components of the energy budgets are quite similar in magnitude. The ratio of the components to each other are nearly the same; for example, the dissipation by vertical mixing is about 2.5 times that due to horizontal mixing in both models. Thus, for a given intensity, the models are energetically quite similar.

It is interesting to compare the circular mean vertical cross sections of the asymmetric model with the corresponding vertical sections of the symmetric model at a time when the storms are approximately of the same intensity. Mean cross sections for the tangential wind, radial wind, and temperature departure at 222 hr of the asymmetric model storm are shown in figure 7, and may be compared with the analogous sections at 89 hr for the symmetric model shown in figure 8. These times correspond to the maximum intensity in both models.

The symmetric model shows a somewhat more intense circulation that is concentrated nearer to the origin. The maximum wind of about 50 m/s occurs at 30 km. The mean cross sections for the asymmetric storm show a larger circulation with mean maximum winds of about 45 m/s occurring at 45 km. These differences are probably related to the differences in effective horizontal resolution which result from the different horizontal grids

The better resolution of the pressure gradient force by the staggered grid in the symmetric model produces the maximum inflow at a smaller radius (60 compared to 105 km). Through the conservation of angular momentum, this increased inflow at a smaller radius produces a higher maximum wind speed.

Aside from the differences caused by different resolutions near the center, the symmetric storm structure is very similar to the azimuthal mean asymmetric storm structure. Both storms show an eye with sinking motion at the center, both show nearly identical outflow patterns, and both have a maximum temperature anomaly of 6°C in the upper troposphere and a weak cold core in the lower troposphere. These similarities tend to support the validity of utilizing symmetric models to study many of the essential features of tropical cyclones.

## 4. SUMMARY AND CONCLUSIONS

This paper compares the asymmetric model hurricane (described by ART) with an axially symmetric analog. Significant differences in the sequence of events in the histories of the two model storms are found. The symmetric model quickly reaches a maximum intensity corresponding to a moderate hurricane, and then begins to slowly decrease in intensity. The asymmetric system, on the other hand, initially reaches a much weaker intensity, remains in a nearly steady state for a time, and then shows a second period of intensification. The differences in intensity during the first 100 hr are related to differences in horizontal resolution produced by the staggered grid used with the symmetric model. The staggered grid provides for a better resolution of the intense pressure gradient near the center of the storm than does the unstaggered grid of the asymmetric model, and confirms that increased resolution near the center of the asymmetric grid is necessary. These facts suggest that the asymmetric model should be recoded in a staggered grid similar to that used for the symmetric model.

The second period of intensification that starts at 120 hr in the asymmetric model does not occur in the symmetric analog. This fact supports the conclusion reached in ART that the development of large-scale asymmetries at about 100 hr is closely associated with the subsequent intensification.

Although the life cycles of the two model storms were quite different, the azimuthally averaged structure of the asymmetric storm at maximum intensity appeared to differ from the structure obtained with the symmetric analog mainly in details attributable to the differences in resolution produced by the staggering of horizontal grid points in the symmetric analog. This similarity tends to support the adequacy of symmetric models in investigating many important aspects of tropical cyclone structure.

### ACKNOWLEDGMENTS

The authors thank Messrs. Robert Carrodus, John Lundblad, and Glenn Frye for the drafting of the figures; Mr. Charles True for the photography; and Mrs. Mary Jane Clarke for typing the manuscript.

### REFERENCES

Anthes, Richard Allen, "A Diagnostic Model of the Tropical Cyclone in Isentropic Coordinates," *ESSA Technical Memorandum* ERLTM-NHRL 89, U.S. Department of Commerce, National Hurricane Research Laboratory, Miami, Fla., Apr. **1970**, 147 pp.

Anthes, Richard Allen, Rosenthal, Stanley L., and Trout, James W., "Preliminary Results From an Asymmetric Model of the Tropical Cyclone," *Monthly Weather Review*, Vol. 99, No. 10, Oct. **1971**, pp. 744–758.

Hawkins, Harry F., and Rubsam, Daryl T., "Hurricane Hilda, 1964: II. Structure and Budgets of the Hurricane on October 1, 1964," *Monthly Weather Review*, Vol. 96, No. 9, Sept. **1968**, pp. 617–636.

Hebert, Paul J., and Jordan, Charles L., "Mean Soundings for the Gulf of Mexico Area," *National Hurricane Research Project Report* No. 30, U.S. Department of Commerce, Weather Bureau, Miami, Fla., Apr. **1959**, 10 pp.

Kurihara, Yoshio, and Holloway, J. Leith, Jr., "Numerical Integration of a Nine-Level Global Primitive Equations Model Formulated by the Box Method," *Monthly Weather Review*, Vol. 95, No. 8, Aug. **1967**, pp. 509–530.

Matsuno, Taroh, "Numerical Integrations of the Primitive Equations by a Simulated Backward Difference Method," *Journal of the Meteorological Society of Japan*, Ser. 2, Vol. 44, No. 1, Tokyo, Feb. **1966**, pp. 76–84.

Miller, Banner I., "On the Momentum and Energy Balance of Hurricane Helene (1958)," *National Hurricane Research Project Report* No. 53, U.S. Department of Commerce, Weather Bureau, Miami, Fla., Apr. **1962**, 19 pp.

Ooyama, Katsuyuki, "Numerical Simulation of the Life-Cycle of Tropical Cyclones," *Journal of the Atmospheric Sciences*, Vol. 26, No. 1, Jan. **1969**, pp. 3–40.

Pamlén, Erik H., and Riehl, Herbert, "Budget of Angular Momentum and Kinetic Energy in Tropical Cyclones," *Journal of Meteorology*, Vol. 14, No. 2, Apr. **1957**, pp. 150–159.

Phillips, Norman A., "A Coordinate System Having Some Special Advantages for Numerical Forecasting," *Journal of Meteorology*, Vol. 14, No. 2, Apr. **1957**, pp. 184–185.

Riehl, Herbert, and Malkus, Joanne S., "Some Aspects of Hurricane Daisy, 1958," *Tellus*, Vol. 13, No. 2, Stockholm, Sweden, May **1961**, pp. 181–213.

Rosenthal, Stanley L., "Numerical Experiments With a Multilevel Primitive Equation Model Designed to Simulate the Development of Tropical Cyclones: Experiment I," *ESSA Technical Memorandum* ERLTM-NHRL 82, U.S. Department of Commerce, National Hurricane Research Laboratory, Miami, Fla., Jan. **1969**, 36 pp.

Rosenthal, Stanley L., "A Circularly Symmetric Primitive Equation Model of Tropical Cyclone Development Containing an Explicit Water Vapor Cycle," *Monthly Weather Review*, Vol. 98, No. 9, Sept. **1970**, pp. 643–663.

Shuman, Frederick G., and Stackpole, John D., "Note on the Formulation of Finite Difference Equations Incorporating a Map Scale Factor," *Monthly Weather Review*, Vol. 96, No. 3, Mar. **1968**, pp. 157–161.

Smagorinsky, Joseph, Manabe, Syukuro, and Holloway, J. Leith, Jr., "Numerical Results From a Nine-Level General Circulation Model of the Atmosphere," *Monthly Weather Review*, Vol. 93, No. 12, Dec. **1965**, pp. 727–768.

Sundqvist, Hilding, "Numerical Simulation of the Development of Tropical Cyclones With a Ten-Level Model, Part 1," *Tellus*, Vol. 22, No. 4, Stockholm, Sweden, **1970**, pp. 359–390.

Yamasaki, Masanori, "A Tropical Cyclone Model With Parameterized Vertical Partition of Released Latent Heat," *Journal of the Meteorological Society of Japan*, Vol. 46, No. 3, Tokyo, June **1968**, pp. 202–214.

[*Received November 17, 1970; revised February 5, 1971*]